Catalysis Letters 33 (1995) 357–368

Electron microscopy studies of vanadium phosphorus oxide catalysts derived from $VOPO_4 \cdot 2H_2O$

Christopher J. Kiely [a], Sujata Sajip [a], Ian J. Ellison [b], Maria T. Sananes [c], Graham J. Hutchings [b] and Jean-Claude Volta [c]

[a] *Department of Materials Science and Engineering, University of Liverpool, PO Box 147, Liverpool, L69 3BX, UK*

[b] *Leverhulme Centre for Innovative Catalysis, Department of Chemistry, University of Liverpool, PO Box 147, Liverpool, L69 3BX, UK*

[c] *Institut de Recherches sur la Catalyse, CNRS, 2 Avenue Albert Einstein, 69626 Villeurbanne Cedex, France*

Received 24 January 1995; accepted 19 April 1995

An electron microscopy study of vanadium phosphorus oxide (VPO) catalysts is reported. The catalyst precursor $VOHPO_4 \cdot 0.5H_2O$ was prepared from $VOPO_4 \cdot 2H_2O$ using isobutanol as the reducing agent. The catalyst was then fully activated by heating for ca. 75 h under reaction conditions (385°C, GHSV 1000 h^{-1}, 1.5% butane in air). Scanning electron microscopy studies demonstrated that a topotactic transformation occurs between the precursor and the final catalyst. Transmission electron microscopy experiments revealed that there were three distinctive morphologies present in the final catalyst; namely (i) rosette shaped clusters composed of $(VO)_2P_2O_7$ crystallites, (ii) crystalline platelets of α_{II}-$VOPO_4$ and (iii) disordered platelets exhibiting surface patches of $(VO)_2P_2O_7$. This latter morphology corresponds to the disordered remnants of hemihydrate particles which have only partially transformed to $(VO)_2P_2O_7$. The $(VO)_2P_2O_7$ platelets were found to be the majority phase making up more than 95% of the volume fraction.

Keywords: vanadium phosphorus oxide; *n*-butane oxidation; high resolution electron microscopy

1. Introduction

Vanadium phosphate catalysts represent one of the most studied selective oxidation catalysts and there have been extensive studies published [1] since Bergmann and Frisch [2] first indicated the efficacy of these materials for the oxidation of *n*-butane to maleic anhydride. Although well studied, there remains some uncertainty as to the nature and role of the vanadium phosphate phases present in the active catalysts. Many studies have involved the use of non-equilibrated catalysts [1] since the catalyst requires ca. 1000 h activation under reaction conditions to achieve a stabilised catalyst performance. Some researchers favour a single compound, $(VO)_2P_2O_7$, to be the sole active phase [3] and have indicated that the presence of

other phases may be due to incomplete activation. However, a number of recent studies on VPO catalysts prepared in aqueous media have indicated the additional presence of α_{II}-, δ- and γ-$VOPO_4$ [4]. Furthermore, during the course of the activation of the hemihydrate precursor, $VOHPO_4 \cdot 0.5H_2O$, these $VOPO_4$ phases appear simultaneously with $(VO)_2P_2O_7$ and this corresponds to the initial formation of maleic anhydride, demonstrating that the active catalyst requires both V^{4+} and V^{5+} in close proximity [5].

To date, there have been very few TEM studies of vanadium phosphorus oxides reported [6–8], but these did not directly relate to activated catalysts of industrial interest. One reason for this paucity of TEM studies on these materials is the extreme sensitivity of vanadium phosphorus oxides to structural damage in the electron beam. In particular, the catalyst precursor $VOHPO_4 \cdot 0.5H_2O$ is very beam sensitive. In this paper we demonstrate that, by carefully controlling the observation conditions and using video recording techniques, meaningful microstructural information on the activated catalysts can be obtained. We provide clear evidence concerning the structure of VPO catalysts which have been derived from the reduction and dehydration of $VOPO_4 \cdot 2H_2O$ using isobutanol, followed by activation under reaction conditions for ca. 75 h. This new preparation route has recently been reported [9] to produce activated catalysts with similar specific activities but much higher surface areas than materials prepared by the more usual non-aqueous solvation route.

2. Experimental

2.1. CATALYST PREPARATION AND TESTING

The catalyst precursor ($VOHPO_4 \cdot 0.5H_2O$) was prepared by reacting V_2O_5 (12 g) with aqueous H_3PO_4 (115.5 g, 85%) in H_2O (24 ml/g solid) under reflux for 8 h. The resultant $VOPO_4 \cdot 2H_2O$ phase was recovered by filtration and subsequently washed with a little water. This dihydrate phase (4 g) was then refluxed for 21 h with predried isobutanol (80 ml) and the resultant blue solid was recovered by filtration. This material was then dried in air (110°C, 16 h) and later confirmed by powder X-ray diffraction to be $VOHPO_4 \cdot 0.5H_2O$.

The catalyst precursor (1.5 g, as powder) was evaluated for the oxidation of *n*-butane using a standard laboratory microreactor. The precursor, $VOHPO_4 \cdot 0.5H_2O$, was transformed into the active catalyst in situ in the reactor by heating under controlled conditions (385°C, 1000 h^{-1}, 1.5% *n*-butane in air) for 75 h. Products were analysed using on-line gas chromatography and carbon mass balances were typically 98–102% for all data cited. The final activated catalyst was cooled in situ in the reactor in dry nitrogen and stored under vacuum until needed for microanalysis.

2.2. CATALYST CHARACTERISATION

Catalyst samples were characterised before and after catalyst testing using powder X-ray diffraction. The resultant solid was also subjected to detailed microstructural analysis using a combination of scanning electron microscopy, transmission electron microscopy and high resolution electron microscopy.

An Hitachi S-2460-N scanning electron microscope was also employed to obtain topographical information on the specimens. Samples suitable for transmission electron microscopy analysis were prepared by dispersing the catalyst powder onto a lacey carbon film supported on a copper mesh grid. TEM observations were made in a Jeol 2000EX high resolution electron microscope operating at 200 kV. This instrument has been fitted with a low-light-level TV camera and a frame averaging system to allow us to use very low illumination conditions. This latter requirement was essential for beam sensitive vanadium phosphorus oxide compounds. Images were recorded on S-VHS videotape, individual frames from which could be captured into a Macintosh Quadra computer for subsequent enhancement and analysis.

3. Results

3.1. CATALYST PERFORMANCE FOR *n*-BUTANE OXIDATION

The catalytic performance was monitored during the transformation of the catalyst precursor to the final catalyst in situ in the reactor. The selectivity to maleic anhydride and the *n*-butane conversion were observed to steadily increase with reaction time, reaching a plateau after ca. 30 h. After this time, a steady catalyst performance is observed with an *n*-butane conversion of 62% and maleic anhydride selectivity of 64% [4]. Following reaction, the catalyst was cooled slowly in an inert atmosphere prior to removal from the reactor for electron microscopy studies. The BET surface areas of the catalyst precursor and the final catalyst were determined to be 32 and 43 $m^2\ g^{-1}$ respectively.

Powder X-ray diffraction patterns from the precursor $VOHPO_4 \cdot 0.5H_2O$ phase (fig. 1a), in which the 220 reflection is the dominant feature, are indicative of a highly textured morphology. The XRD spectrum from the final activated catalyst (shown in fig. 1b) is consistent with the formation of $(VO)_2P_2O_7$ only. It is interesting to note that "200" reflection in fig. 1b is considerably broadened due to a combination of (i) the presence of several overlapping peaks (200, 102, 040) with very similar plane spacings (0.386, 0.406 and 0.414 nm respectively) and (ii) the platelike morphology of the catalyst. The fact that no characteristic lines from any $VOPO_4$ phases are present in fig. 1b suggests that such phases are either completely absent or are present at levels below the detectability level of the XRD technique.

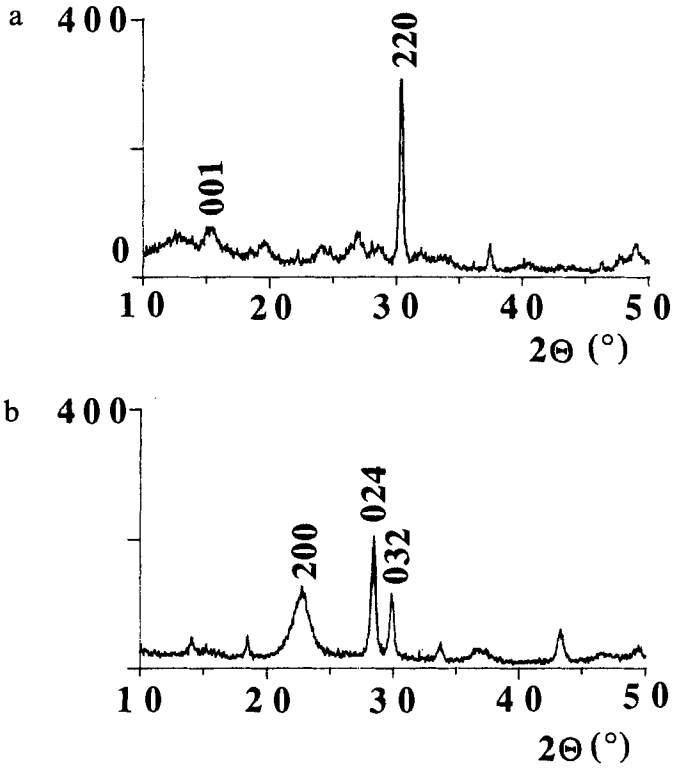

Fig. 1. Powder X-ray diffraction patterns obtained from (a) the precursor $VOHPO_4 \cdot 0.5H_2O$ phase and (b) the final activated catalyst (showing characteristic $(VO)_2P_2O_7$ reflections only).

3.2. ELECTRON MICROSCOPY STUDIES

The catalyst precursor and the final catalyst were examined by scanning electron microscopy as shown in figs. 2a and 2b respectively. The precursor material consists of plate-like crystals (less than 0.1 μm thick) which are arranged into characteristic rosette shaped clusters of 1–3 μm in diameter. The final activated catalyst has a very similar morphology, although considerably more isolated platelets were also present, as shown in fig. 2b. The retention of the characteristic rosette structure is consistent with a topotactic transformation of the precursor to the final catalyst which has been previously reported [10].

TEM examination of the final catalyst also showed a combination of rosette shaped clusters and isolated platelets as shown, labelled p, in fig. 3. Selected area diffraction patterns obtained at normal incidence to the isolated platelets always gave a characteristic square geometry pattern (fig. 4a), which could be indexed to the [001] zone axis of α_{II}-$VOPO_4$. This phase has a tetragonal structure (space group P4/n) with a and c parameters of 0.601 and 0.443 nm respectively [11]. It was also possible, using our low-light-level imaging system, to record characteristic axial [001] α_{II}-$VOPO_4$ lattice images from such platelets. The micrograph in fig. 4b

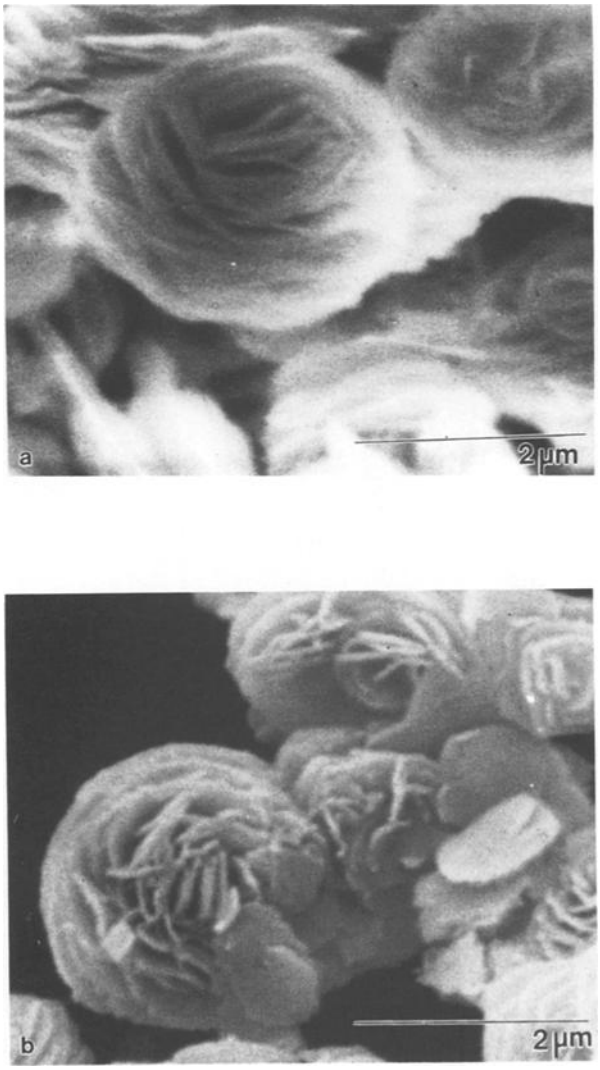

Fig. 2. Scanning electron micrographs showing the morphology of (a) the catalyst precursor and (b) the final activated catalyst.

shows such an image in which the 200 and 020 lattice spacings (0.3 nm) are resolved. Even under the low dose imaging conditions employed, such α_{II}-$VOPO_4$ lattice images only persisted for 1 or 2 s before complete amorphization occurred. These α_{II}-$VOPO_4$ platelets accounted for about 3–4 vol% of the sample.

The rosette-type agglomerates, which at ~95 vol% constitute the majority phase, have also been studied by HREM. Lattice images, such as that shown in fig. 5a, were obtained from the tips of individual "edge-on" crystallites. Analysis of fringe spacings (0.386 nm) ($d_{\bar{2}00}$) and 0.414 nm (d_{004})) and intersection angles

Fig. 3. Bright field transmission electron micrograph of the activated catalyst showing rosette-shaped clusters and one of the less common individual isolated platelets.

(90°) has allowed us to identify the image as the [010] projection of $(VO)_2P_2O_7$. This phase has an orthorhombic crystal structure with *a*, *b* and *c* parameters of 0.773, 0.957, and 1.657 nm respectively [12]. A Fourier transform (FT) obtained from this lattice image (see inset in fig. 5a) corresponds closely to the [010] diffraction pattern expected from $(VO)_2P_2O_7$. In addition, an HREM image of one of these crystallites, obtained in a direction normal to the platelet, is presented in fig. 5b. The fringe structure (crossed 1.66 and 0.96 nm fringes with a 90° intersection angle) is consistent with that expected from the [100] projection of $(VO)_2P_2O_7$. This is confirmed by the accompanying FT. Hence the rosette type structures are made up from agglomerates of $(VO)_2P_2O_7$ platelets that are preferentially exposing (100) crystal planes.

Two other features concerning the $(VO)_2P_2O_7$ phase are also worthy of mention at this point. Firstly, $(VO)_2P_2O_7$ is slightly more resistant to electron beam damage than α_{II}-$VOPO_4$, typically lasting about 5–10 s before amorphisation under our illumination conditions. Secondly, as shown in fig. 6, small fragments of $(VO)_2P_2O_7$ (typically less than 400 nm in size) are sometimes seen to be supported in random orientations on the α_{II}-$VOPO_4$ platelets. These fragments have presumably spalled-off from the rosette clusters during catalyst activation. In fact, there

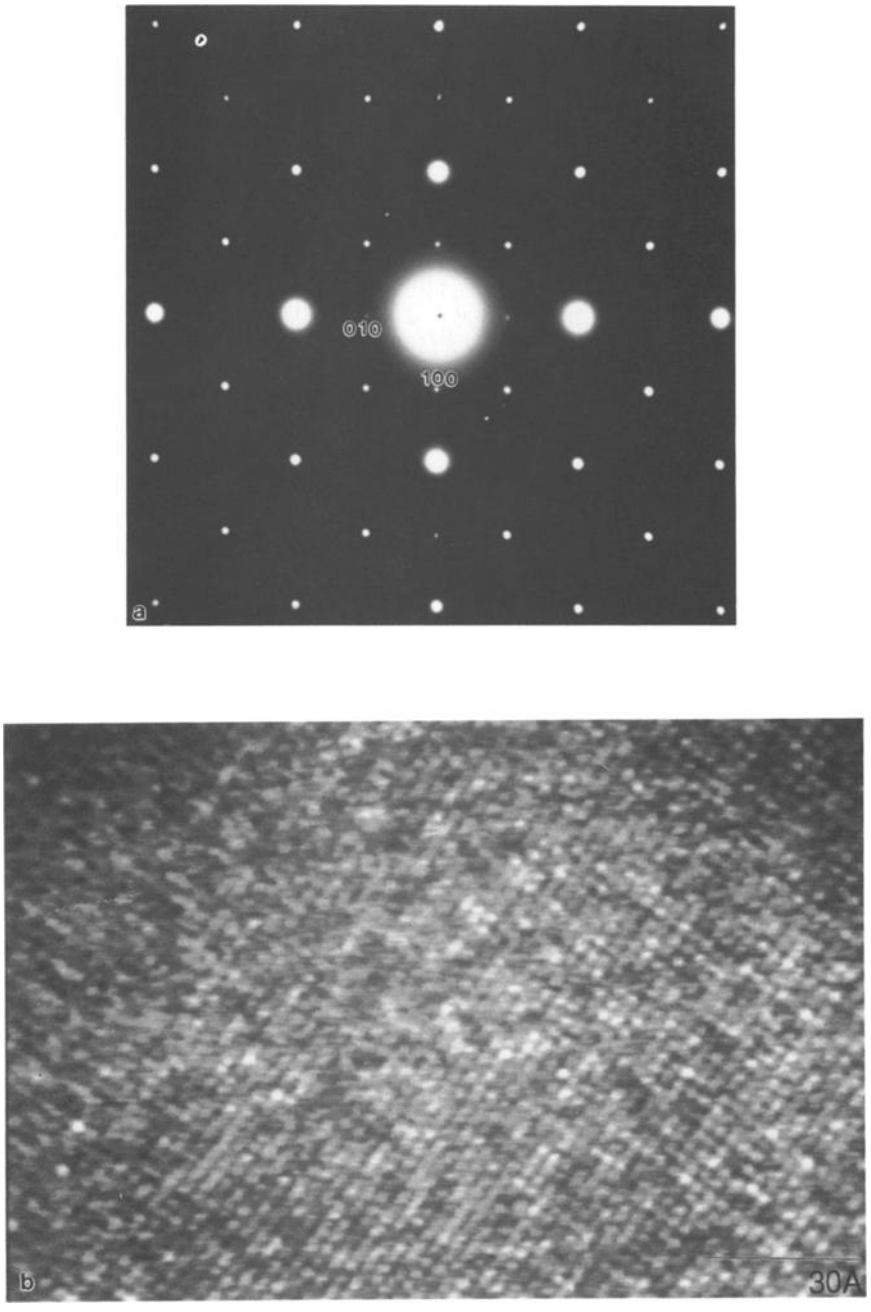

Fig. 4. (a) A selected area diffraction pattern obtained from a direction normal to the isolated platelet which can be indexed as [001] α_{II}-$VOPO_4$. A typical HREM image obtained from this zone axis is shown in (b).

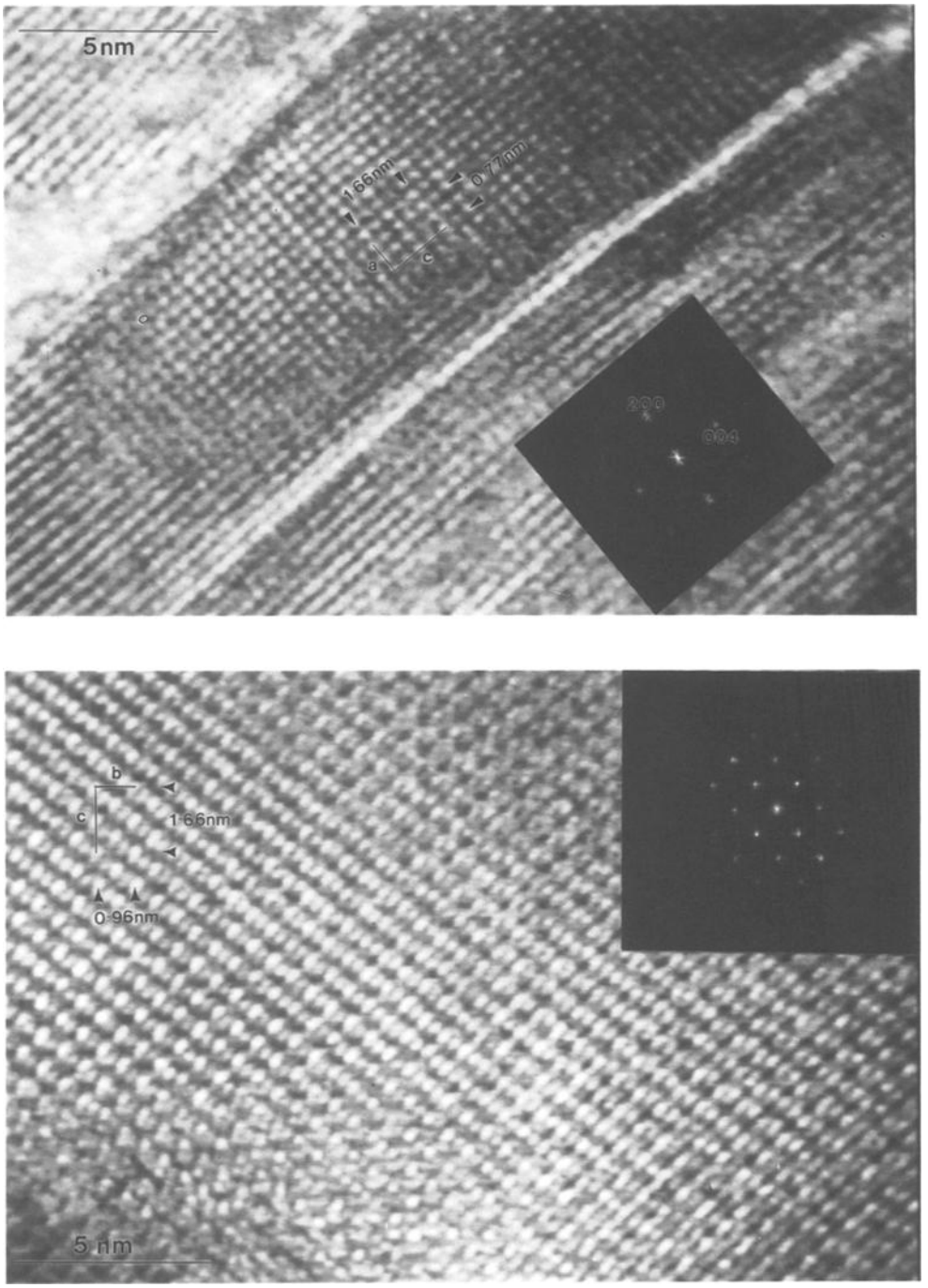

Fig. 5. HREM images obtained (a) edge-on and (b) normal to a platelet incorporated in one of the rosette type clusters. These correspond to the [010] and [100] projections of $(VO)_2P_2O_7$ respectively.

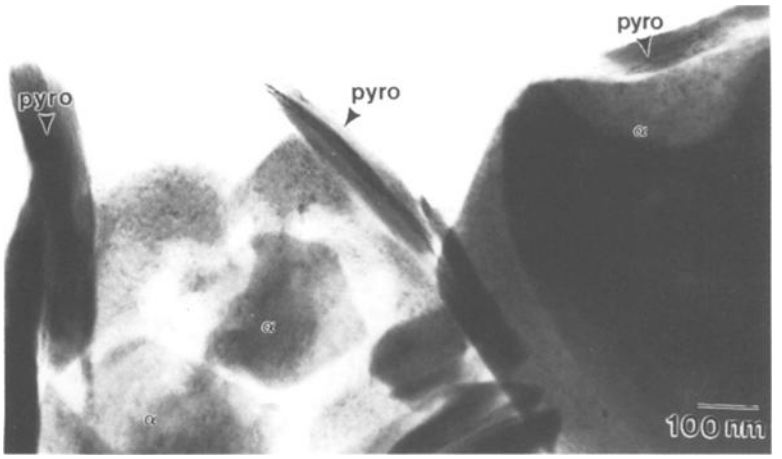

Fig. 6. Bright field image showing spalled fragments of $(VO)_2P_2O_7$ which are supported on α_{II}-$VOPO_4$ platelets.

is supporting evidence for spalling in fig. 5a, where the edge-on $(VO)_2P_2O_7$ platelet appears to be "cleaving" between two adjacent (100) planes.

A third, much rarer, platelet-type morphology has also been observed in the activated sample. These platelets, which are typically about 0.1–0.2 μm in size, are more beam sensitive and structurally disordered than either of the previously described $(VO)_2P_2O_7$ or α_{II}-$VOPO_4$ phases. Elongated raft-like patches of a second phase were always seen on the surface of these platelets. The typical dimensions of these patches were about 15 × 5 nm. In addition, on any platelet the long dimensions of the patches were aligned suggesting that an orientation relationship exists between the support and the second phase. When observed by HREM, the surface patches were always found to be much more stable (i.e. a 5–10 s lifetime) under the electron beam than the underlying platelet. A typical HREM image of a surface patch is shown in fig. 7b in which a 0.38 nm ($d_{\bar{2}00}$) set of fringes run parallel to the long axis and a 0.32 nm ($d_{02\bar{4}}$) set of fringes run in the perpendicular direction. These fringe separations and intersection angles correspond reasonably well with those expected from the [021] projection of $(VO)_2P_2O_7$. Hence, we suspect that the third morphology may correspond to the remnants of a hemihydrate particle which has only partially transformed to $(VO)_2P_2O_7$.

4. Discussion

The detailed electron microscopy characterisation of the final active catalyst, prepared from $VOHPO_4 \cdot 0.5H_2O$ derived from $VOPO_4 \cdot 2H_2O$, indicates that several distinct vanadium phosphorus oxide phases are present. We have deduced that the activated catalyst mainly contains $(VO)_2P_2O_7$, along with minor amounts of

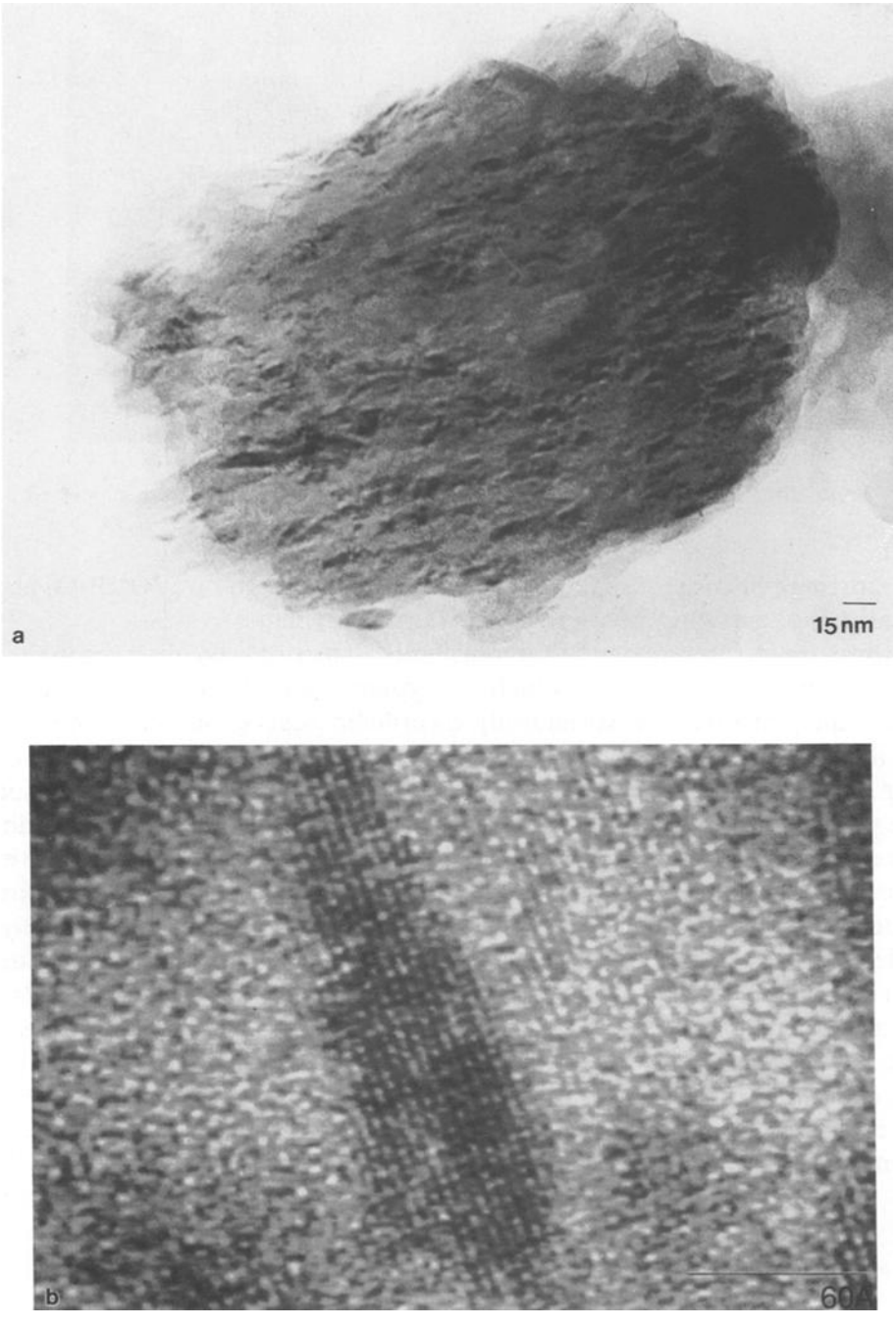

Fig. 7. (a) Bright field micrograph showing elongated raft-like patches of a second phase on the surface of a disordered platelet. Lattice fringe structure can be imaged in these surface patches (see (b)) which can be indexed to the [021] projection of $(VO)_2P_2O_7$.

α_{II}-$VOPO_4$ and partially transformed material. Previous studies have suggested that the presence of $VOPO_4$ phases is indicative that the catalyst has not been subjected to sufficient equilibration under the reaction conditions [3]. However, in our studies catalysts have been activated for sufficient reaction time using appropriate reaction conditions and the catalyst was found to have a stable catalytic performance with the activity and selectivity expected for a non-promoted catalyst derived from $VOHPO_4 \cdot 0.5H_2O$ (specific activity = 1.19 mol maleic anhydride $m^{-2}\ h^{-1}$) [12].

A number of previous studies have indicated that a combination of phases is beneficial. For example, an early patent disclosure reported that catalysts containing α_{II}-$VOPO_4$ in addition to $(VO)_2P_2O_7$ were more active and the increase in activity was related to the amount of α_{II}-$VOPO_4$ phase present [13]. Further evidence to confirm that the combination of $(VO)_2P_2O_7$ and α_{II}-$VOPO_4$ is beneficial is provided by the observations that pure α_{II}-$VOPO_4$ is not particularly selective for maleic anhydride formation [14,15], although it is active for butane oxidation, and that pure $(VO)_2P_2O_7$ is not very active [16]. Hence, it is not unreasonable to suppose that the combination of a V^{4+} phase ($(VO)_2P_2O_7$) and a V^{5+} phase ($VOPO_4$), which are both present after 50–100 h activation, is an important pre-requisite in the development of a final catalyst that gives an optimal performance after ca. 1000 h activation.

The precise nature of the active site in vanadium phosphorus oxide catalysts is still a matter of much controversy. In situ Raman experiments [5] have demonstrated that, during the course of the activation of the hemihydrate precursor, $VOPO_4$ and $(VO)_2P_2O_7$ phases appear simultaneously and this event coincides with the initial formation of maleic anhydride. It is thus highly probable that the active catalyst requires the presence of both V^{4+} and V^{5+} ions in close proximity. Electron microscopy studies may indeed allow us to make some progress in identifying the true nature of the active site. Gai and Kourtakis [8] have very recently performed some severe reductions of the $(VO)_2P_2O_7$ phase in situ in the electron microscope and observed surface modification accompanied by the formation of extended shear defects. These latter defects, if present under normal reaction conditions, could possibly be sites where V^{4+} and V^{5+} ions co-exist. We are currently attempting similar environmental cell experiments in which we are employing reaction conditions much closer to those encountered under typical catalyst activation situations. In addition, we are studying materials that contain some $VOPO_4$ as well as $(VO)_2P_2O_7$ phases as is the situation encountered in typical non-promoted VPO catalysts.

Acknowledgement

We thank the European Community Human Capital Mobility Programme (contract CHRX-CT92-0065) and EPSRC for financial support.

References

[1] G. Centi, Catal. Today 18 (1994) 1.
[2] R.L. Bergman and N.W. Frisch, US Patent 3293268 (1968), assigned to Princeton Chemical Research.
[3] J.R. Ebner and M.R. Thompson, Catal. Today 18 (1994) 51.
[4] G.J. Hutchings, R. Olier, M.T. Sananes and J.C. Volta, Stud. Surf. Sci. Catal. 82 (1994) 213.
[5] G.J. Hutchings, A. Desmartin-Chomel, R. Olier and J.C. Volta, Nature 368 (1994) 41.
[6] H.S. Horowitz, C.M. Blackstone, A.W. Sleight and G. Teufer, Appl. Catal. 38 (1988) 211.
[7] P. Ruiz, Ph. Bastians, L. Cassin, R. Reuse, L. Daza, D. Acosta and B. Delmon, Catal. Today 16 (1993) 39.
[8] P.L. Gai and K. Kourtakis, Science 267 (1995) 661.
[9] G.J. Hutchings, Catal. Today 18 (1994).
[10] J.W. Johnson, D.C. Johnson, A.J. Jacobson and J.F. Brady, J. Am. Chem. Soc. 106 (1984) 8123.
[11] E. Bordes, P. Courtine and J.W. Johnson, J. Solid State Chem. 55 (1984) 270.
[12] Yu.E. Gorbunova and S.A. Linde, Dokl. Akad. Nauk. SSSR 245 (1979) 584.
[13] G.J. Hutchings and R. Higgins, UK Patent 1601121 (1981), assigned to Imperial Chemical Industries.
[14] L. Morselli, F. Trifirò and L. Urban, J. Catal. 75 (1982) 112.
[15] Y. Zhang-Lin, M. Forissier, R.P. Sneeden, J.C. Vedrine and J.C. Volta, J. Catal. 145 (1994) 256.
[16] T.P. Moser and G.L. Schrader, J. Catal. 92 (1985) 216.